



Fabrication and characterization of 3D printed biocomposite scaffolds based on PCL and zirconia nanoparticles

Qifan Wang¹ · Zhiyong Ma^{2,3} · Ying Wang¹ · Linna Zhong⁴ · Wenjia Xie⁴

Received: 16 June 2020 / Accepted: 8 August 2020 / Published online: 24 August 2020
© Zhejiang University Press 2020

Abstract

The application of three-dimensional printed polymer scaffolds in repairing bone defects is a promising strategy. Among them, polycaprolactone (PCL) scaffolds are widely studied due to their good processability and controlled degradation rate. However, as an alternative graft for repairing bone defects, PCL materials have poor hydrophilicity, which is not conducive to cell adhesion and growth. In addition, the poor mechanical properties of PCL materials cannot meet the strength required to repair bone defects. In this paper, nano-zirconium dioxide (ZrO₂) powder is embedded in PCL material through a melt-mixing process, and a regular grid scaffold is constructed by 3D printing. The embedding of nanometer zirconium dioxide powder improves the hydrophilicity and water absorption of the composite scaffold, which is conducive to cell adhesion, proliferation and growth and is beneficial to the exchange of nutrients. Therefore, the PCL/ZrO₂ composite scaffold showed better biological activity in vitro. At the same time, the PCL/ZrO₂ composite material system significantly improves the mechanical properties of the scaffold. Among them, compared with the pure PCL scaffold, the Young's modulus is increased by about 0.4 times, and the compressive strength is increased by about 0.5 times. In addition, the osteogenic differentiation results also showed that the PCL/ZrO₂ composite scaffold group showed better ALP activity and more effective bone mineralization than the pure PCL group. We believe that the 3D printed PCL/ZrO₂ composite scaffold has certain application prospects in repairing bone defects.

Keywords 3D printing · Bone tissue engineering · Biocomposite scaffold · Zirconium dioxide · Hydrophilicity

Introduction

The high incidence of bone disease has led to an increased demand for alternatives to conventional bone grafts used to repair or reconstruct bone defects. The preparation of biomaterial-based bone tissue engineering scaffolds through additive manufacturing methods is a promising solution [1].

The ideal bone tissue engineering scaffold should be able to repair bone defects and restore bone tissue function to the greatest extent. Therefore, the scaffold must have microstructure characteristics and mechanical properties close to human bones and have good biocompatibility and bone conductivity [2].

3D printing has the advantages of high precision, rapid prototyping and preparation of complex structures, which can meet the needs of personalized medicine and has a wide range of applications in tissue engineering [3, 4]. 3D printing is becoming popular due to its precise control of the aperture and structure of the prototype [5–8]. In bone tissue engineering, the three-dimensional structure of the scaffold can provide a good environment for cell adhesion and proliferation. Regular porous structures (pore size, porosity and pore interconnection) and layered porous (macropores, micropores) have facilitated the transportation of nutrients and the migration of cells to the scaffold [9–12].

In bone tissue engineering scaffolds, synthetic polymers and bioceramics are widely used due to their good

✉ Zhiyong Ma
02641@zjhu.edu.cn

¹ College of Mechanical Engineering and Mechanics, Ningbo University, Ningbo 315211, Zhejiang, People's Republic of China

² School of Engineering, Huzhou University, Huzhou 313000, Zhejiang, People's Republic of China

³ Huzhou Aixiante Electronic Technology co., LTD., Huzhou 313000, Zhejiang, People's Republic of China

⁴ Department of Prosthodontics, West China Hospital of Stomatology, Sichuan University, Chengdu 610000, Sichuan, People's Republic of China

biocompatibility and mechanical properties [13]. Polycaprolactone (PCL) is a polymer scaffold material with good processability and controlled degradation rate [14], but its mechanical properties and biocompatibility are poor, so PCL is generally not used alone as bone tissue scaffolds. A common solution is to add bioceramic materials, such as hydroxyapatite and tricalcium phosphate, to the PCL to improve mechanical properties, enhance cell proliferation activity and promote bone formation [15, 16]. In recent years, some researchers have used ceramic materials/PCL to prepare artificial bone scaffolds, such as Jeon et al. [17] prepared melt extrusion 3D printing PCL and silanized modified silica composite scaffold has good mechanical properties and significant cell proliferation and calcium mineralization properties. Khoshroo et al. [18] incorporated titanium dioxide nanotubes into PCL scaffolds to improve the mechanical and biological properties of bone tissue engineering scaffolds. Yeo et al. [19] on the collagen/HA and PCL composite scaffold prepared the electrospinning method, and the cells showed better proliferation and osteogenic differentiation ability. However, the mechanical properties of these composite scaffolds are still relatively small and cannot meet the required bone strength.

Existing research shows that tissue engineering scaffold with hydrophilic surface is more conducive to cell adhesion [20]. Zirconium dioxide (ZrO_2) nanopowder can enhance the hydrophilicity of polymer materials [21]. At the same time, the elastic modulus of ZrO_2 is matched with human bones, has high mechanical strength and fracture toughness and has excellent osseointegration and can be combined with living bone [22]. As other methods, some research groups have attempted to study bone defect healing on PCL/ ZrO_2 composite materials. For example, Catauro et al. [23, 24] immersed the prepared PCL/ ZrO_2 composite film in simulated body fluid to form a hydroxyapatite layer on the surface, proving the good biological activity of PCL/ ZrO_2 composite; the sol–gel method synthesizes PCL/ ZrO_2 composite material and prepares seamless film by dip coating technology to improve the biological activity of titanium-based materials. Based on the existing research, the PCL/ ZrO_2 composite system has good biological activity and can promote bone formation.

However, the researchers did not combine this composite material system with 3D printing technology to build a regular grid scaffold to provide better and more controllable nutrition supply and substance exchange. We hope to add nano-zirconia particles to PCL materials to form a PCL/ ZrO_2 composite materials system. The good hydrophilicity of nano-zirconia particles can improve the biocompatibility of composite materials. At the same time, the good mechanical properties of the zirconia material are used to improve the mechanical properties of the composite material so that the composite material can meet the mechanical properties

required by the bone scaffold. Finally, combined with 3D printing, a composite scaffold with a regular grid structure was constructed to be used in bone tissue engineering repair.

This paper combines the 3D printing technology and uses the good hydrophilicity and high mechanical strength of ZrO_2 materials to solve the problem of poor hydrophilicity and mechanical properties of PCL materials. At the same time, the PCL material has good processability and controllable degradation rate. We combine the hybrid process and melt printing technology to prepare PCL/ ZrO_2 composite scaffold, obtain a controllable three-dimensional pore structure. For the prepared scaffold, we evaluated the composition, surface morphology, hydrophilicity and compression resistance of the scaffold. In order to observe the effect of the scaffold on cells (cell adhesion, proliferation, morphology and differentiation), mouse embryo osteoblast precursor cells (MC3T3 cells) were used to examine the prepared composite scaffold.

Experiment

Preparation of PCL/ ZrO_2 composite scaffold

To prepare the composite scaffold, two processes are used: the material mixing process and the fusion 3D printing process (Fig. 1a). First, PCL (molecular weight 70,000, melting point 60 °C, Jinan Daigang Biological Engineering Co., Ltd., China) was melted at 120 °C, and then, zirconium dioxide (Suzhou Dingan Technology Co., Ltd., China) powder was added to the molten PCL and mixed the two materials to achieve uniformity. Second, the uniformly mixed composite material is placed in a stainless steel barrel. Then, a 22G (400 μ m) nozzle was used to extrude the molten PCL composite with zirconium dioxide embedded. The air pressure and nozzle movement speed during printing are 350 kPa and 6 mm/s, respectively. The barrel temperature is 105 ± 5 °C. Finally, the rheological test simulates the printing status and further refines the printing temperature. In this work, PCL/ ZrO_2 composite scaffolds with 5, 10 and 20 wt % zirconium dioxide content were designed as PZ5, PZ10 and PZ20, respectively.

Characterization of composite scaffold

The composite material was detected using an X-ray powder diffractometer (XRD6100, Shimadzu, Japan) and scanned at a speed of 10 deg/min with a scanning range of 5°–55°. A contact angle measuring instrument (JY-82B, Chengdu Leading Instrument Co., Ltd., China) was used to measure the water contact angle (WCA) of the composite scaffold. The same volume composite scaffold ($\phi 6.8 \times 2.8$ mm) was weighed before and after immersion in distilled water (take

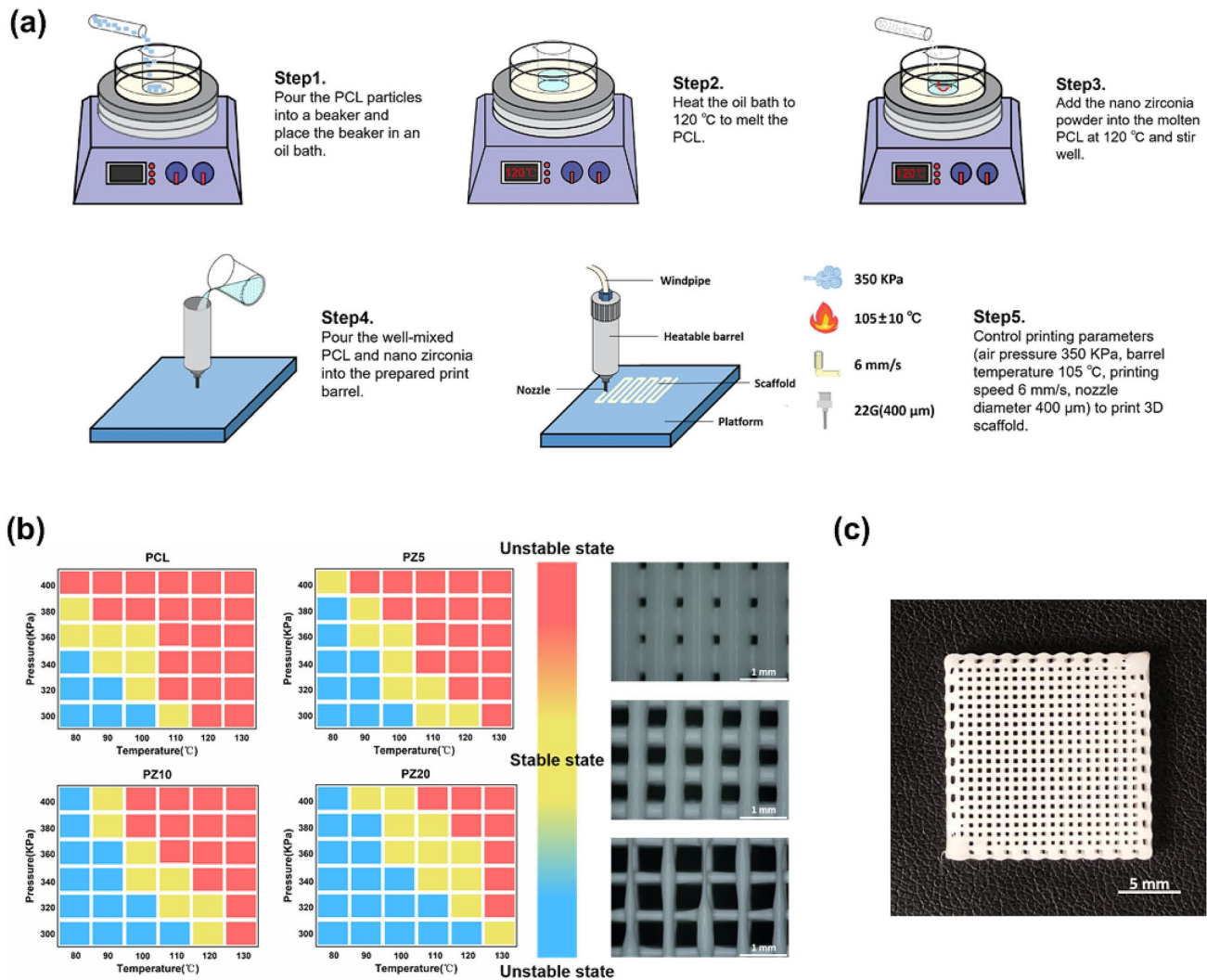


Fig. 1 **a** PCL/ZrO₂ composite material mixing process and printing diagram. **b** Extrusion 3D printing process window, depending on air pressure and temperature. **c** 3D printed scaffold

1, 3 and 12 h, respectively) to calculate the water absorption. The percentage increase in water absorption is calculated as $(\%) = (M1 - M0)/V0 \times 100$, where $M1$ is the mass of the scaffold after water absorption, $M0$ is the original mass of the scaffold before water absorption and $V0$ is the volume of the scaffold.

The surface morphology of the fabricated composite scaffold was observed using a scanning electron microscope (SEM, TCS-SP2, Leica, Germany), and the pore size and fiber size of the composite scaffold were calculated using microscopic analysis. A 3D optical profilometer (NewView9000, Zygo, USA) was used to observe the three-dimensional topography of the manufactured composite scaffold surface. Use the water injection method to calculate the porosity of the scaffold. The scaffold porosity percentage is calculated as $(\%) = (M2 - M0)/\rho V0 \times 100$, where $M2$ is the mass of the scaffold after water injection, $M0$ is the original

mass of the scaffold before water injection, ρ is the density of water and $V0$ is the volume of the scaffold.

Cut the composite scaffold sample into a cylinder ($\phi 6.8 \times 2.8$ mm) and use a material test system (MTS, WH-5000 N, Weiheng Testing Instrument Co., Ltd., China) to perform compression test. After preloading 0.454 kg (1 lb), at a compression speed of 10 mm/min, the amount of compression is 50% (1.4 mm) of the sample height dimension, record the stress–strain curve of the scaffold, take the 25% strain to calculate the compressive strength of the scaffold and calculate Young's modulus of the scaffold.

In vitro cell culture

The scaffold was cut into a rectangular parallelepiped (5.6 mm \times 5.6 mm \times 2.8 mm) and soaked in medical alcohol for 2 h for disinfection and then placed in a 48-well plate

and soaked in MEM medium overnight. After removing the medium, each well was inoculated with 500 μ l of MC3T3 cell suspension with a density of 4×10^4 and incubated at 37 °C. for 6 h in a 5% CO₂ environment. After replacing the well plate, the culture was continued and maintained in MEM containing 10% fetal bovine serum With 1% antibiotic–antifungal agent, the medium was changed every 48 h.

Cell survival test

In order to confirm the survival status of the cells on the scaffold, the working solution (2 μ M calcein AM, 8 μ M PI) was prepared and mixed thoroughly. The cell-bearing scaffold was removed on 1, 3 and 7 days and washed with 1 \times PBS three times, then add working solution and incubate for 20 min, add 1 \times PBS and wash once add anti-fluorescence quencher and observe the surface of the cell-bearing scaffold using a scanning laser confocal microscope (FV3000, Olympus, Japan) to analyze the cell survival rate. Calcein AM labels live cells and emits green fluorescence, and propidium iodide (PI) labels dead cells and emits red fluorescence.

Cytoskeletal detection

In order to detect the growth status of the cells on the scaffold, the cells were continuously cultured on the scaffold for 7 days, and the cell-bearing scaffold was taken out on the seventh day, washed 3 times with 1 \times PBS, treated with 0.5% Triton-X-100 for 10 min, washed with 1 \times PBS 3 times, add phalloidin to incubate for 0.5 h in the dark, wash 3 times in 1 \times PBS, then add DAPI incubation for 10 min in the dark, wash 3 times in 1 \times PBS, add anti-fluorescence quencher and store at 4 °C in the dark. The surface of the cell-bearing scaffold was observed using a scanning laser confocal microscope (FV3000, Olympus, Japan). Analyze the growth of MC3T3 cells.

Cell adhesion rate and proliferation

In order to measure the adhesion rate of cells on the scaffold, the cells were cultured in the well plate with the scaffold for 6 h and then transfer the scaffold to the new well plate culture. The cells in the original well plate were digested with trypsin and counted. The calculation percentage of cell adhesion rate is (%) = $(N_0 - N_1)/N_0 \times 100$, where N_0 is the number of initially seeded cells and N_1 is the number of remaining cells in the original well plate.

In order to evaluate the proliferation of cells on the scaffold, the proliferation detection reaction solution was prepared according to the ratio of 50 μ l cck8: 1000 μ l medium, and the reaction solution was added to the well plate on days 1, 3 and 7, respectively, and incubated at 37 °C under 5% CO₂ environment. After 3 h, the absorbance at OD450nm

of the reaction solution was measured. Imagej software was used to analyze DAPI-labeled nuclei in cytoskeleton staining pictures on days 1, 3 and 7 to calculate the number of cells.

ALP staining and alizarin red S staining

To confirm the differentiation level of cell culture, it was determined by measuring the release of p-nitrophenol alkaline phosphatase (ALP) activity in p-nitrophenyl phosphate (p-NPP). After the cells-bearing scaffolds were continuously cultured for 10 days, osteogenic induction medium (0.1 mM dexamethasone + 10 mM β -glycerophosphate disodium salt solution + 50 μ g/ml L-ascorbic acid) was used for induction. After 1 and 3 days of induction, remove the scaffold and wash the scaffold with 1 \times PBS, add 4% paraformaldehyde for 15 min at room temperature, wash 3 times with 1 \times PBS, add ALP staining solution and incubate for 2 h at room temperature, wash the scaffold with 1 \times PBS and then pass the Microscope (JSZ6S, Nuoxu Microelectronics Co., Ltd., China) to observe the staining of the surface of the scaffold.

Calcium mineralization of cells was determined by alizarin red S staining. After the cells-bearing scaffolds were continuously cultured for 10 days, osteogenic induction medium (0.1 mM dexamethasone + 10 mM β -glycerophosphate disodium salt solution + 50 μ g/ml L-ascorbic acid) was used for induction. After 7 and 14 days of induction, remove the scaffold and wash the scaffold with 1 \times PBS, add 95% ethanol to fix at room temperature for 15 min, wash 3 times with 1 \times PBS, add Alizarin Red S staining solution and stain for 30 min at room temperature, wash the scaffold with 1 \times PBS and then pass an optical microscope (JSZ6S, Nuoxu Microelectronics Co., Ltd., China) to observe the staining of the scaffold surface.

Statistical analysis

All data in the experiment were expressed in the form of mean \pm standard deviation (SD), and statistical analysis was performed using analysis of variance ($n = 3$). A single asterisk (*) indicates $0.01 < P < 0.05$, and there are statistical differences between the groups. Double asterisks (**) indicate $0.001 < P < 0.01$, and there are statistically significant differences between the groups. Three asterisks (***) indicate $p < 0.001$, and there are extremely significant statistical differences between the groups.

Results and discussion

Preparation process of composite scaffold

Containing a suitable uniform pore structure can provide a good and stable growth environment for cell growth, while

having certain mechanical properties. We use the melt-mixing process and 3D printing method to effectively prepare the scaffold and control the stable fiber output by controlling the extrusion air pressure and the barrel temperature. Figure 1b shows the printable window for mixing materials in various ratios at different pressures and temperatures. The blue area is an unstable fiber with too large pores; the extruded 3D printed fiber is thick under the red area, and the pore size is too small; the yellow area is a printable window with stable fibers and suitable pore size. Figure 1c shows a picture of the scaffold printed by the air pressure and temperature parameters in the yellow area.

In order to make the printed PCL/ZrO₂ composite scaffold with four different ratios having the same structure, it provides good guarantee for subsequent experiments. The rheological test verifies the printing performance of the material. Figure 2a shows through rheological shear thinning that as the shear rate continues to increase, the viscosity of the material decreases accordingly. The state of the material during 3D printing by pneumatic extrusion was simulated. Figure 2b shows the rheological temperature curve as the temperature continues to increase, the viscosity of the material decreases accordingly. It is verified that the viscosity of the printed material is controlled by the temperature control. The viscosity of PCL composites added with ZrO₂ nanopowder is significantly higher than that of pure PCL materials. By analyzing the rheological temperature curve and

combining the printable window of the material, the printing parameters of the material are further determined, and the printing temperature of the material with different proportions under the same viscosity is selected (PCL: 96.5 °C, PZ5: 100.5 °C, PZ10: 105 °C, PZ20: 114 °C). Finally, four kinds of scaffolds for subsequent experiments were prepared. We prepared two different layers of composite scaffolds, eight layers and 12 layers, respectively. The 12-layer scaffold is used for mechanical testing, and the eight-layer scaffold is used for other experimental tests.

Material properties of composite scaffold

Figure 2b shows the XRD pattern of pure PCL, ZrO₂ and composite materials (PZ5, PZ10 and PZ20). The XRD pattern of pure PCL has two strong peaks at $2\theta \approx 21.4^\circ$ and 23.8° . They are, respectively, related to the (110) and (200) reflections of the polyethylene crystal structure [25]. All composite groups showed PCL peaks. The peaks corresponding to ZrO₂ nanopowders are at $2\theta \approx 30.3^\circ$, 35.2° and 50.3° . The XRD diffraction pattern of PCL/ZrO₂ composite material proved that ZrO₂ nanopowder was successfully embedded into the PCL scaffold.

Hydrophilicity is the most important characteristic of biomedical scaffolds because they control the attachment, diffusion and proliferation of primary cells [26, 27]. To observe the effect of mixed ZrO₂ nanopowders on the hydrophilicity

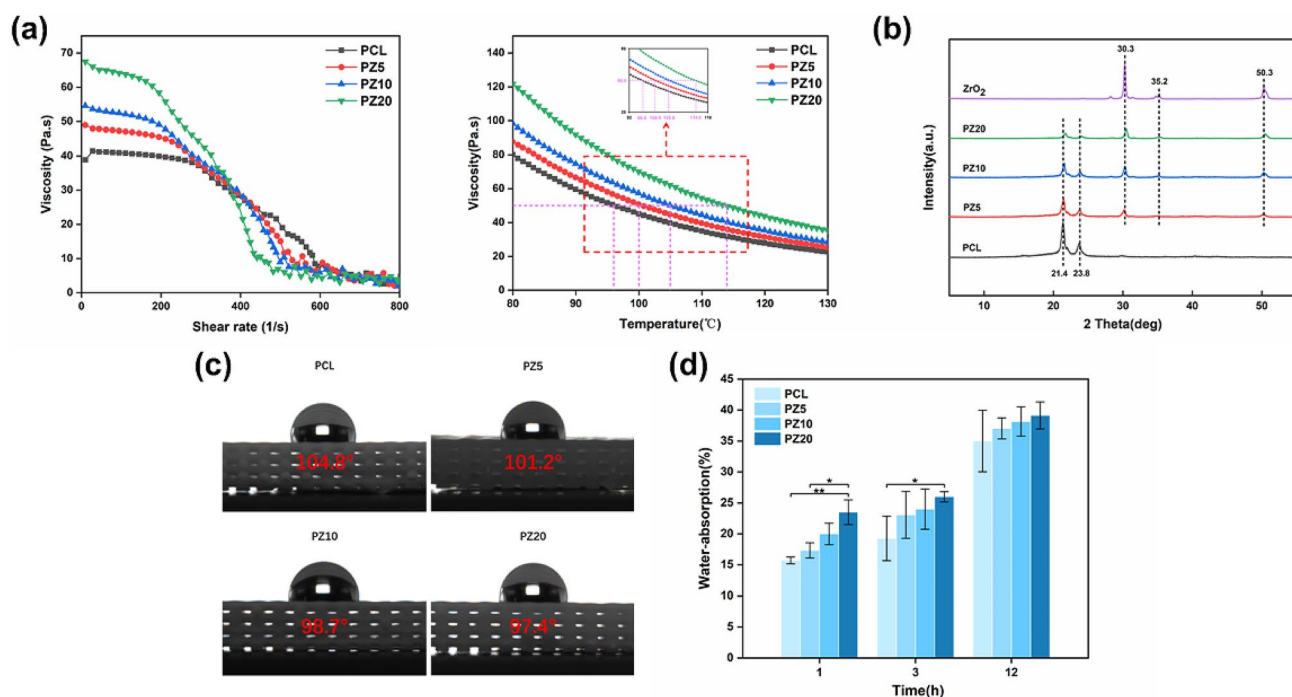


Fig. 2 a Rheological shear thinning and temperature–viscosity curve. b X-ray diffraction (XRD) spectroscopy. c Optical image of scaffold contact angle results. d Comparison of water absorption capacity after immersion in distilled water for 1, 3 and 12 h ($n=3$)

of the scaffold, we dropped 10 μl of water onto each sample. As shown in Fig. 2c, with increasing ZrO_2 content, the initial WCA of droplets on various composite scaffolds showed gradually lower values compared to pure PCL. It is proved that the PCL scaffold mixed with ZrO_2 nanopowder has better hydrophilicity.

Water absorption capacity is the basic requirement of the scaffold, and because proper absorption is conducive to nutrient exchange and deterioration, it can help maintain metabolic function and promote cell proliferation. As shown in Fig. 2d, the composite scaffold showed significantly higher water absorption capacity than pure PCL within 3 h. And there is a statistically significant difference in the water absorption of PZ20 compared with pure PCL at 1 h and a statistical difference at 3 h. We believe that the embedding of ZrO_2 nanopowders helps the scaffold to absorb water.

Morphology of composite scaffold

Biomaterial scaffolds with pore diameters $> 300 \mu\text{m}$ show better osteogenic effects because they provide cell penetration, blood vessel formation and hyperoxia [28, 29].

In addition, scaffolds with interconnected pores and high porosity can provide cells with the required physical geometry and support proper vascularization of ingrowth tissue [30]. For this purpose, we designed a scaffold with a pore size of approximately $450 \mu\text{m}$ and a porosity of approximately 45%. As shown in the surface and cross-sectional SEM images of the scaffold shown in Fig. 3a and c, the prepared scaffold has a relatively uniform pore size and fiber size, and the scaffold has an interconnected pore structure. The pore size and fiber size of the scaffold were calculated by microscopic analysis, and the porosity of the scaffold was measured by the water injection method, as shown in Table 1. The final result shows that the prepared scaffold

Table 1 Pore size, fiber diameter and porosity of the pure PCL and composite scaffolds

	PCL	PZ5	PZ10	PZ20
Pore size (μm)	461.9 ± 9.9	459.0 ± 6.8	462.7 ± 7.5	459.2 ± 6.1
Fiber size (μm)	352.8 ± 5.2	355.1 ± 4.3	353.7 ± 4.2	354.9 ± 4.3
Porosity (%)	46.8 ± 2.3	46.2 ± 2.0	47.0 ± 1.7	46.2 ± 1.6

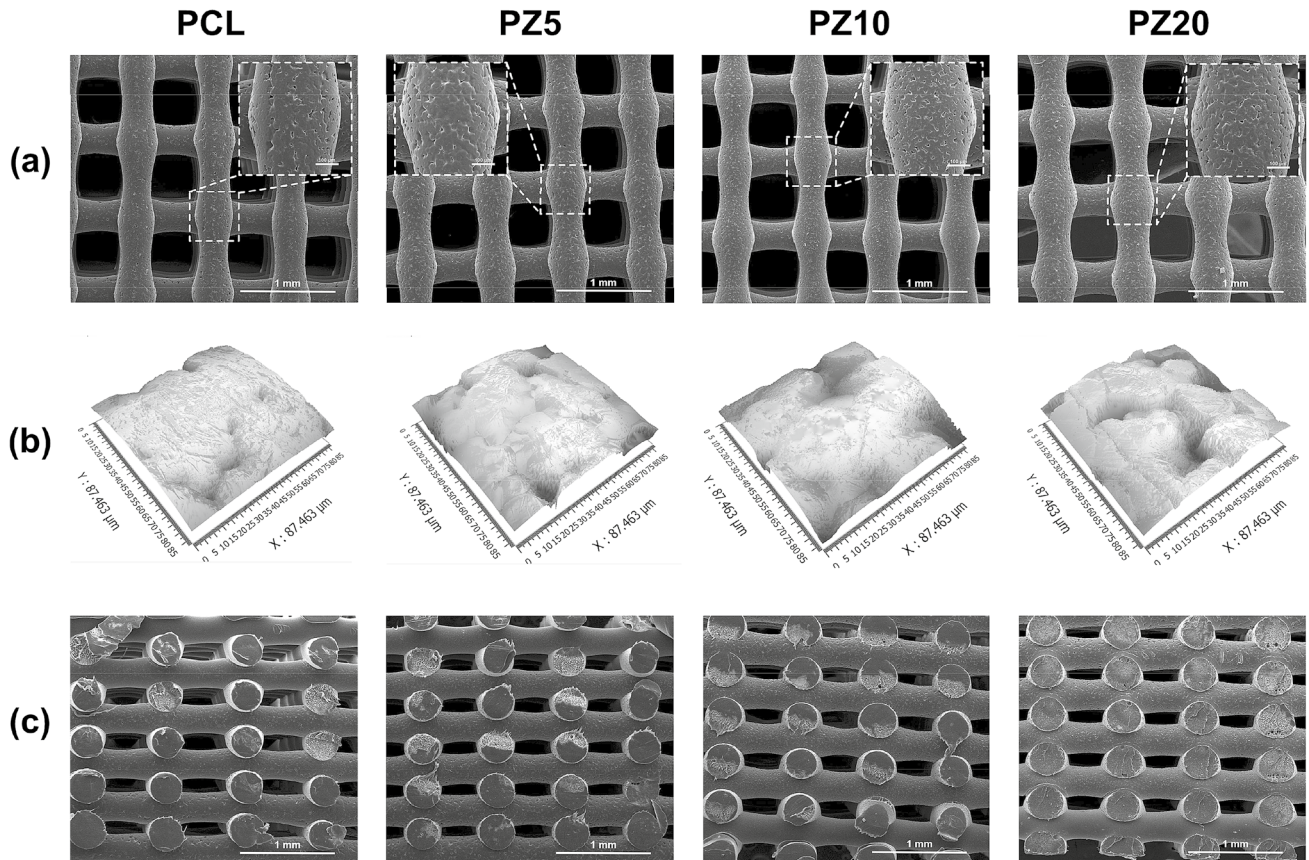


Fig. 3 a SEM images of the surface pore structure of the pure PCL and composite scaffolds. b 3D optical profiler observes the images showing the roughened surface of scaffolds. c SEM images of the lateral cross-sectional view

achieves the expected pore size and porosity, and there was no significant difference between several groups.

Studies have reported that roughness has a positive effect on cell differentiation and gene expression [31, 32]. As shown in Fig. 3b, the 3D optical profiler observes the image of the surface of the scaffold. As the ZrO_2 content increases, the surface of the composite scaffold shows a rough surface pattern.

Mechanical properties

In bone tissue engineering, the mechanical properties of 3D scaffolds are crucial to their biological properties. The mechanical properties of the scaffold depend on its material composition and porosity. The four sets of scaffolds we designed have the same porosity, and the mechanical properties of PCL scaffolds are improved by trying to add

ZrO_2 nanopowder. As shown in Fig. 4a, the compression test is performed by a material test system.

Figure 4b, c and d shows the stress–strain curves, compressive strength and Young’s modulus of pure PCL and composite (PZ5, PZ10 and PZ20) scaffolds, respectively. Compared with pure PCL scaffolds, the stress–strain curve of composite material is significantly increased, and the compressive strength and Young’s modulus are also significantly improved. In addition, the compressive strength and Young’s modulus of PZ20 and pure PCL scaffolds are extremely significant statistical different. Compared with the pure PCL scaffold, the compressive strength of the PZ20 scaffold is increased by about 50%, and the Young’s modulus is increased by about 40%. Based on these results, we believe that the embedding of ZrO_2 nanopowder helps to improve the mechanical properties of the scaffold.

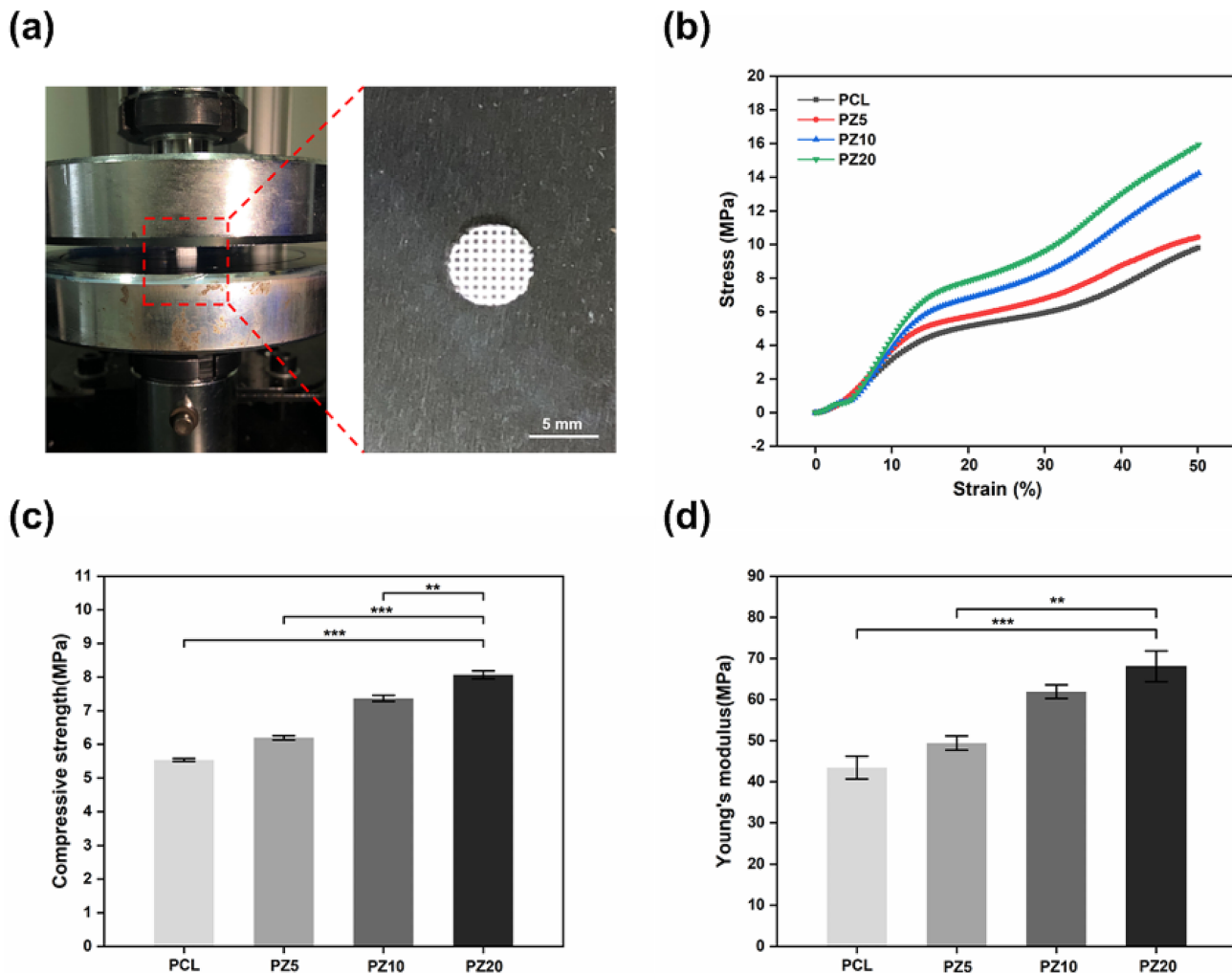


Fig. 4 **a** Compressed optical images of the scaffold. **b** The stress–strain curve of the scaffolds. **c** Compare the compressive strength of the scaffolds and **d** Young’s modulus ($n=3$)

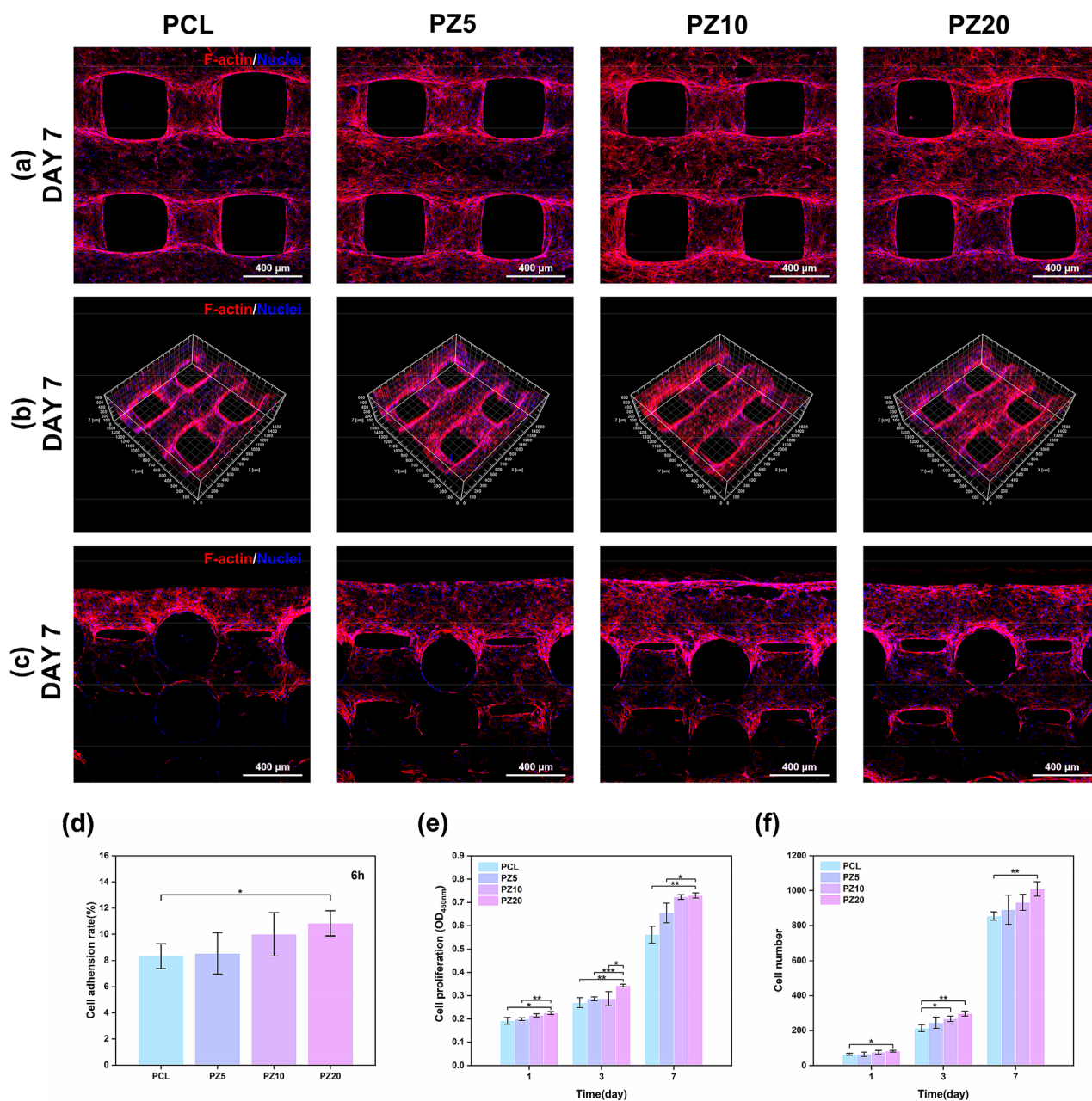


Fig. 6 **a** Surface of pure PCL and composite scaffold nuclei (blue) and F-actin (red), **b** three-dimensional and **c** cross-sectional laser confocal microscope images at 1, 3 and 7 days. **d** Cell adhesion rate of

scaffolds at 6 h. **(e)** CCK-8 test on pure PCL and composite scaffold and **f** cell count at 1, 3 and 7 days ($n=3$)

clearly observed according to the content of ZrO_2 . As shown in Fig. 6c, by observing the cross section of the scaffold on the seventh day of culture, it can be clearly observed that as the ZrO_2 content increases, the cells grow longer along the longitudinal direction of the scaffold. These results prove that the ZrO_2 nanopowder embedded in the scaffold helps cell adhesion, proliferation and growth.

As shown in Fig. 6d, by counting the number of cells remaining after 6 h of hole replacement, the adhesion

rate of cells on the scaffolds of pure PCL and composite materials (PZ5, PZ10, and PZ20) was calculated. Compared with the pure PCL scaffold, the cell adhesion rate on the PZ20 scaffold has been statistically improved. As shown in Fig. 6e and f, the absorbance of the test solution of the cells on the scaffolds of each group at 1, 3 and 7 days at 450 nm was tested by the CCK-8 experiment and microanalysis, and the cell's quantity. Compared with the pure PCL scaffold, the absorbance of the test solution

of cells on the PZ20 scaffold was improved at 1, 3 and 7 days. And there was a statistically significant difference between the PZ20 and PCL scaffold groups at 3d and 7d. The number of cells on the PZ20 scaffold on days 1, 3 and 7 increased compared with the pure PCL scaffold. And there was a statistically significant difference between the PZ20 and PCL scaffold groups at 3d and 7d. The above results indicate that the PZ20 group showed better cell adhesion rate and better cell proliferation. We believe that the embedding of ZrO₂ nanopowders provides an environment conducive to cell adhesion and proliferation due to the material properties of hydrophilicity and roughness.

Osteogenic differentiation

ALP activity is a general marker of bone mineralization and represents an important biochemical marker in the early stages of bone formation [33]. In this study, we observed the expression of ALP osteogenic markers during the differentiation of MC3T3 cells in the composite scaffold. As shown in Fig. 7a and b, after continuous culture of the cell-bearing scaffold for 10 days, ALP staining was tested by inducing the scaffold for 1 and 3 days. In the results, compared with the pure PCL scaffold, with the increase in ZrO₂ content, the ALP expression of the composite scaffold (PZ5, PZ10 and PZ20) has a trend of increasing sequentially. Based on this result, we speculate that the embedding of ZrO₂ nanopowder is beneficial to induce cell differentiation.

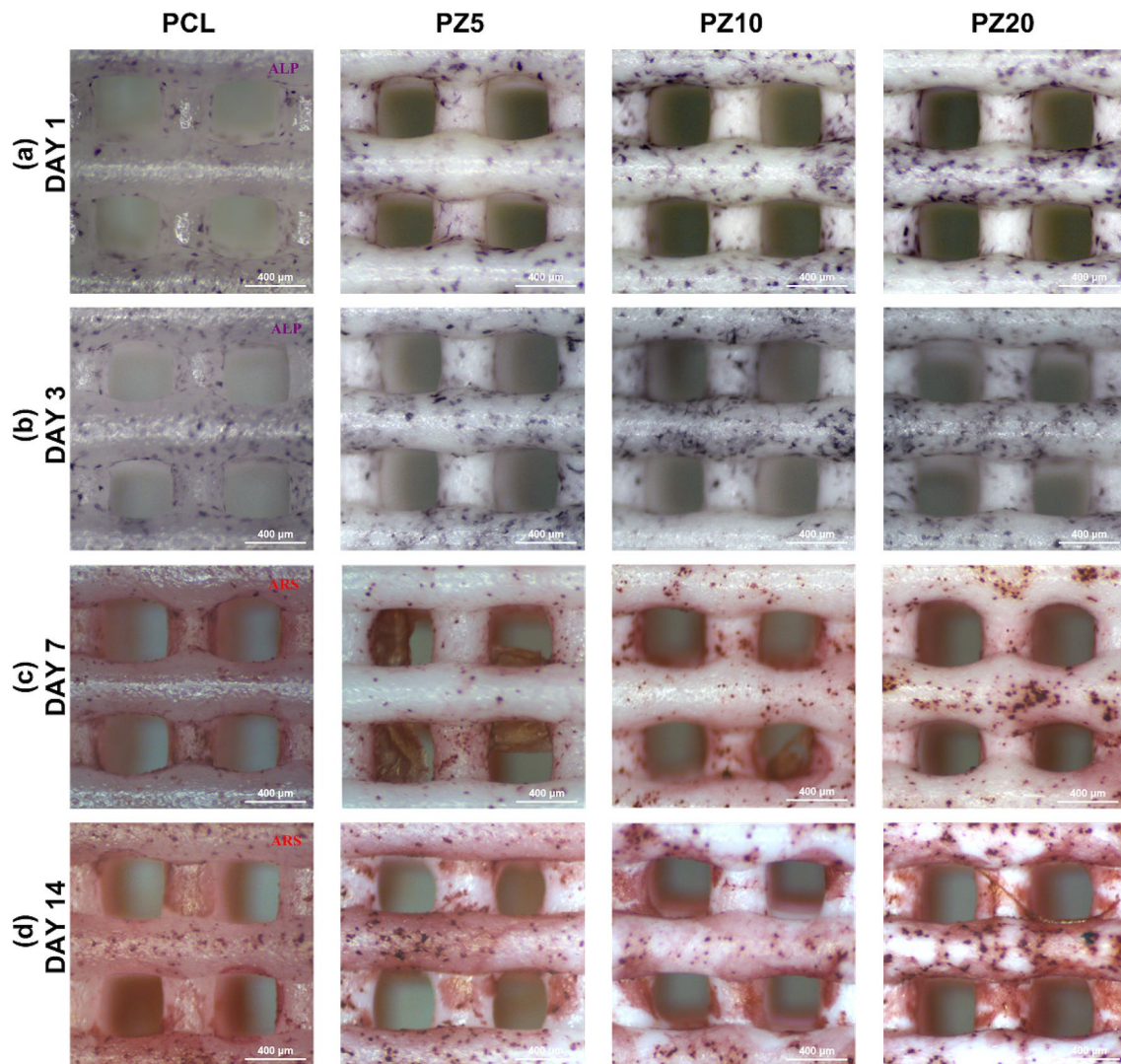


Fig. 7 a ALP staining diagrams of pure PCL and composite scaffolds induced for 1 and b 3 days. c ARS staining diagrams of scaffolds induced for 7 and d 14 days

As shown in Fig. 7c and d, the alizarin red staining results of 7 days and 14 days were further induced with the cell-bearing scaffolds continuously cultured for 10 days. As a result, the increase in ZrO₂ increased the amount of calcium deposits produced, especially on PZ20. These results show that when we embed ZrO₂ nanopowder in the scaffold, the calcium deposition of MC3T3 cells increased and osteogenic differentiation was achieved.

Conclusion

In this study, we manufactured a PCL/ZrO₂ composite scaffold mixed with various ratios (5, 10 and 20 wt%) of ZrO₂ nanopowders by melt-mixing and extrusion 3D printing. The PCL/ZrO₂ composite scaffold shows significant physical and chemical properties. Compared with the pure PCL group, the PCL/ZrO₂ composite scaffold group has higher hydrophilicity and good water absorption capacity. At the same time, the PCL/ZrO₂ composite scaffold group has better mechanical properties, including improved compressive strength and enhanced Young's modulus. Moreover, the increased hydrophilicity of the composite scaffold also affects the biological activity, which is more conducive to cell adhesion and nutrient transport. Therefore, compared with the pure PCL group, the PCL/ZrO₂ composite scaffold group showed better cell adhesion, proliferation and growth. The osteogenic differentiation results also showed that the PCL/ZrO₂ composite scaffold group showed better ALP activity and accommodated more effective bone mineralization than the pure PCL group. These results are closely related to the embedding of ZrO₂ nanopowder in the PCL/ZrO₂ composite scaffold. Based on the physical and chemical performance results and biological performance results, the PCL composite scaffold embedded with ZrO₂ nanopowder is a transplant material with great potential for bone tissue regeneration.

Author contributor QW, ZM and YW participated in the study design, data analysis, writing and editing of the manuscript. QW, LZ and WX performed the experimental research and data analysis. All authors have read and approved the final manuscript and, therefore, have full access to all the data in the study and take responsibility for the integrity and security of the data.

Compliance with ethical standards

Conflict of interest The authors declare that they have no conflict of interest.

Ethical approval This study does not contain any studies with human or animal subjects performed by any of the authors.

References

- Tang D, Tare RS, Yang LY et al (2016) Biofabrication of bone tissue: approaches, challenges and translation for bone regeneration. *Biomaterials* 83:363–382
- Kang J, Yanen W, Qinghua W et al (2018) Application of 3D printing technology in bone tissue engineering. *Bio-Des Manuf* 1(3):203–210
- Garrett B (2014) 3D printing: new economic paradigms and strategic shifts. *Global Policy* 5(1):70–75
- He Y, Gu Z, Xie M et al (2020) Why choose 3D bioprinting? Part II: methods and bioprinters. *Bio-Des Manuf* 3(1):1–4
- Gao Q, Niu X, Shao L et al (2019) 3D printing of complex GelMA-based scaffolds with nanoclay. *Biofabrication* 11(3):035006
- Ma L, Li Y, Wu Y et al (2020) 3D bioprinted hyaluronic acid-based cell-laden scaffold for brain microenvironment simulation. *Bio-Des Manuf* 3:164–174
- Chia HN, Wu BM (2015) Recent advances in 3D printing of biomaterials. *J Biol Eng* 9(1):1–14
- Xie C, Gao Q, Wang P, Shao L et al (2019) Structure-induced cell growth by 3D printing of heterogeneous scaffolds with ultrafine fibers. *Mater Des* 181:108092
- Ma H, Chun F, Jiang C et al (2018) 3D-printed bioceramic scaffolds: from bone tissue engineering to tumor therapy. *Acta Biomater* 79:37–59
- Shao L, Gao Q, Xie C et al (2020) Sacrificial microgel-laden bioink-enabled 3D bioprinting of mesoscale pore networks. *Bio-Des Manuf* 3:30–39
- Bose S, Vahabzadeh S, Bandyopadhyay A (2013) Bone tissue engineering using 3D printing. *Mater Today* 16(12):496–504
- Park J, Bauer S, von der Mark K et al (2007) Nanosize and vitality: TiO₂ nanotube diameter directs cell fate. *Nano Lett* 7(6):1686–1691
- Navarro M, Aparicio C, Charles-Harris M, et al (2006) Development of a biodegradable composite scaffold for bone tissue engineering: physicochemical, topographical, mechanical, degradation, and biological properties. *Ordered Polym Nanostruct Surf*
- Bártolo Paulo, Bidanda B (2008) *Bio-materials and prototyping applications in medicine*. Springer, New York
- Qu X, Xia P, He J et al (2016) Microscale electrohydrodynamic printing of biomimetic PCL/nHA composite scaffolds for bone tissue engineering. *Mater Lett* 185:554–557
- Huang B, Caetano G, Vyas C et al (2018) Polymer-ceramic composite scaffolds: the effect of hydroxyapatite and β-tri-calcium phosphate. *Materials* 11(1):129
- HoJun J, Minji L, Seokhwan Y et al (2019) Fabrication and characterization of 3D-printed biocomposite scaffolds based on PCL and silanated silica particles for bone tissue regeneration. *Chem Eng J* 360:519–530
- Khoshroo K, Jafarzadeh Kashi TS, Moztarzadeh F et al (2017) Development of 3D PCL microsphere/TiO₂ nanotube composite scaffolds for bone tissue engineering. *Mater Sci Eng C Mater Biol Appl* 70(Pt 1):586–598
- Yeo MG, Kim GH (2012) Preparation and characterization of 3D composite Scaffolds based on rapid-prototyped PCL/β-TCP struts and electrospun PCL coated with collagen and HA for bone regeneration. *Chem Mater* 24(5):903–913
- Sousa I, Mendes A, Pereira RF et al (2014) Collagen surface modified poly(ε-caprolactone) scaffolds with improved hydrophilicity and cell adhesion properties. *Mater Lett* 134(1):263–267
- Pang RZ, Li X, Li JS et al (2013) In situ preparation and anti-fouling performance of ZrO₂/PVDF hybrid membrane. *Acta Physico-Chim Sin* 29(12):2592–2598

22. Li HC, Wang DG, Chen CZ (2015) Effect of zinc oxide and zirconia on structure, degradability and in vitro bioactivity of wollastonite. *Ceram Int* 41(8):10160–10169
23. Catauro Michelina R, Mariagrazia A et al (2008) Sol-gel processing of drug delivery zirconia/polycaprolactone hybrid materials. *J Mater Sci Mater Med* 19(2):531–540
24. Catauro M, Bollino F, Papale F et al (2014) Biological response of human mesenchymal stromal cells to titanium grade 4 implants coated with PCL/ZrO₂ hybrid materials synthesized by sol-gel route: in vitro evaluation. *Mater Sci Eng C* 45:395–401
25. Kim GH, Yoon H (2008) Effect of an auxiliary electrode on the crystalline morphology of electrospun nanofibers. *Appl Phys Lett* 93(2):310–312
26. Wang YW, Wu Q, Chen GQ (2003) Reduced mouse fibroblast cell growth by increased hydrophilicity of microbial polyhydroxyalkanoates via hyaluronan coating. *Biomaterials* 24(25):4621–4629
27. Terriza A, Vilches-Pérez J et al (2014) Osteoconductive potential of barrier nanoSiO₂ PLGA membranes functionalized by plasma enhanced chemical vapour deposition. *Biomed Res Int* 2014:253590
28. Gotz HE, Muller M, Emmel A et al (2004) Effect of surface finish on the osseointegration of laser-treated titanium alloy implants. *Biomaterials* 25(18):4057–4064
29. Tsuruga E, Takita H, Itoh H et al (1997) Pore size of porous hydroxyapatite as the cell-substratum controls bmp-induced osteogenesis. *J Biochem* 121(2):317–324
30. Karageorgiou V, Kaplan D (2005) Porosity of 3D biomaterial scaffolds and osteogenesis. *Biomaterials* 26(27):5474–5491
31. Carson Thomas H, Joel Collier H, Charles Sfeir S et al (2002) Engineering gene expression and protein synthesis by modulating nuclear shape. *Proc Natl Acad Sci USA* 99:1972–1977
32. Lee KY, Alsberg E, Hsiong S et al (2004) Nanoscale adhesion ligand organization regulates osteoblast proliferation and differentiation. *Nano Lett* 4(8):1501–1506
33. Golub EE, Boesze-Battaglia K (2007) The role of alkaline phosphatase in mineralization. *Curr Opin Orthop* 18(5):444–448